Mechanisms of Zoonotic Severe Acute Respiratory Syndrome Coronavirus Host Range Expansion in Human Airway Epithelium[▽]

Timothy Sheahan,[1] Barry Rockx,[2] Eric Donaldson,[1] Amy Sims,[2] Raymond Pickles,[1,3] Davide Corti,[4] and Ralph Baric[1,2]*

*Department of Microbiology and Immunology, University of North Carolina at Chapel Hill, Chapel Hill, North Carolina[1];
Department of Epidemiology, University of North Carolina at Chapel Hill, Chapel Hill, North Carolina[2];
Cystic Fibrosis/Pulmonary Research and Treatment Center, University of North Carolina at Chapel Hill,
Chapel Hill, North Carolina[3]; and Institute for Research in Biomedicine, Bellinzona, Switzerland[4]*

In 2003, severe acute respiratory syndrome coronavirus (SARS-CoV) emerged and caused over 8,000 human cases of infection and more than 700 deaths worldwide. Zoonotic SARS-CoV likely evolved to infect humans by a series of transmission events between humans and animals for sale in China. Using synthetic biology, we engineered the spike protein (S) from a civet strain, SZ16, into our epidemic strain infectious clone, creating the chimeric virus icSZ16-S, which was infectious but yielded progeny viruses incapable of propagating in vitro. After introducing a K479N mutation within the S receptor binding domain (RBD) of SZ16, the recombinant virus (icSZ16-S K479N) replicated in Vero cells but was severely debilitated in growth. The in vitro evolution of icSZ16-S K479N on human airway epithelial (HAE) cells produced two viruses (icSZ16-S K479N D8 and D22) with enhanced growth on HAE cells and on delayed brain tumor cells expressing the SARS-CoV receptor, human angiotensin I converting enzyme 2 (hACE2). The icSZ16-S K479N D8 and D22 virus RBDs contained mutations in ACE2 contact residues, Y442F and L472F, that remodeled S interactions with hACE2. Further, these viruses were neutralized by a human monoclonal antibody (MAb), S230.15, but the parent icSZ16-S K479N strain was eight times more resistant than the mutants. These data suggest that the human adaptation of zoonotic SARS-CoV strains may select for some variants that are highly susceptible to select MAbs that bind to RBDs. The epidemic, icSZ16-S K479N, and icSZ16-S K479N D22 viruses replicate similarly in the BALB/c mouse lung, highlighting the potential use of these zoonotic spike SARS-CoVs to assess vaccine or serotherapy efficacy in vivo.

Diseases caused by emerging viruses such as human immunodeficiency virus, Ebola virus, influenza virus H5N1, West Nile virus, and dengue virus have had a profound impact on global public health (28). In 2003, a novel coronavirus, severe acute respiratory syndrome coronavirus (SARS-CoV), emerged suddenly as the causative agent of SARS and spread worldwide, causing about 8,000 cases and >700 deaths (3, 17, 41). SARS-CoV most likely evolved from viruses circulating within the Chinese horseshoe bat and other bat species that are believed to be the natural animal reservoirs (18). Within live-animal markets in the Guangdong region of China, it is hypothesized that the close cohabitation of bats and palm civets allowed for subsequent cross-species transmission and amplification of bat strains in civets (9, 18). Palm civets then served as an intermediate host for the subsequent viral evolution of strains that could infect and transmit between humans (18). Clinical data suggest that the sporadic early human SARS-CoV infections were significantly less pathogenic than later ones and that a progressive series of adaptive mutations was necessary for increased human-to-human transmission and the expanding phases of the epidemic (2, 9, 41). Despite initial

reports that civet strains SZ16 and SZ3 could be propagated in cell culture, subsequent studies have indicated that these viruses could not be successfully maintained in culture, thereby hampering our understanding of their pathogenicities and mechanisms of cross-species transmission in humans (19).

Within the past 4 years, multiple newly emerging coronaviruses of human relevance have been identified, highlighting the emerging disease potential of the coronavirus family (35, 41, 50, 53). SARS-CoV and human coronavirus HKU1 are newly emerging members of coronavirus genogroup II, and both cause pneumonic disease in humans, with SARS-CoV being the most pathogenic of the known human coronaviruses (7, 17, 41, 52, 53). Viruses related to the SARS-CoV epidemic strain have recently been found in Chinese horseshoe bats during surveillance of wild animals in Hong Kong (18). Since viruses similar to the epidemic strain have been found circulating within zoonotic pools, there is the potential for yet another reemergence (18). Moreover, a promiscuous RNA-dependent RNA polymerase coupled with high-frequency recombination rates makes the evolution of future human coronavirus pathogens a real possibility (6, 36, 57).

The coronavirus spike glycoprotein (S) is a key determinant of host specificity, and elucidating the molecular mechanisms of viral host expansion may help us understand the events that rendered SARS-CoV pathogenic to humans (16, 24). Virus sequence data isolated throughout the course of the epidemic suggest that the S gene was under heavy positive selection

---

during the early phase of the epidemic but eventually stabilized as the epidemic progressed (2). The S protein is 1,225 amino acids (aa) in length and can be divided into two main functional domains, S1 and S2. The S1 region (aa 17 to 756) contains the receptor binding domain (RBD; aa 318 to 510), while the S2 region (aa 757 to 1225) contains the two heptad repeat regions responsible for viral fusion and a transmembrane domain (aa 1189 to 1227) that anchors S to the viral envelope. SARS-CoV entry into the host cell is mediated by a receptor, angiotensin I converting enzyme 2 (ACE2), and perhaps other coreceptors (15, 22). ACE2 has been detected on the apical surfaces of ciliated cells within the lung epithelia as well as in the kidneys and colon (12). After S and receptor binding, the virus enters the cell by receptor-mediated endocytosis. Cleavage of the SARS-CoV S by cathepsin L within the endosome is required for SARS-CoV infection and precedes fusion (42).

Sequences isolated throughout the initial epidemic from 2002 to 2003 and during the reemergence from 2003 to 2004 chronicle the mutations in S that may have allowed for host expansion. During the epidemic and the reemergence, the early 2003 SARS-CoV animal isolate, SZ16, and the 2004 reemergent human isolate, GD03, were among the most divergent viruses isolated from civets and humans, respectively. SARS-CoV SZ16 was identified in palm civets in live-animal markets within the Guangdong region of China during the epidemic, and its S protein differs from that of the epidemic strain, SARS Urbani, in 18 amino acids, 16 of which reside in the S1 domain. Using pseudotyped viruses, recent work has shown that the mutation of residue 479 within the SZ16 RBD was sufficient to allow for the host range expansion of zoonotic SARS-CoV spike-bearing pseudovirus to infect human cells (21, 24).

In this study, we describe the synthetic construction and characterization of a SARS-CoV chimera bearing a zoonotic SZ16 S protein. Importantly, we find that the mutations acquired during the in vitro evolution of a zoonotic, S-bearing recombinant virus in human airway epithelial (HAE) cells can vary from those that occurred during the epidemic, highlighting the adaptive plasticity of the zoonotic S protein. Also, these data suggest that HAE cells can be used as a model to evaluate the possible avenues of SARS-CoV zoonotic S evolution toward the efficient infection of human cells. Lastly, recombinant viruses bearing zoonotic S proteins replicated efficiently in mice and will serve as a valuable tool in assessing the efficacies of vaccines and therapies.

MATERIALS AND METHODS

Viruses and cells. The recombinant epidemic virus strain "icSARS" (GenBank accession no. AY278741), icSZ16-S (GenBank accession no. AY304488), and the icSZ16-S K479N, icSZ16-S K479N D8, and icSZ16-S K479N D22 mutant strains were propagated on Vero E6 cells as described previously (58). Virus stocks used throughout this study were grown and titers were determined by plaque assays with Vero E6 cells as described previously (58). Vero E6 and delayed brain tumor (DBT) cells were grown in minimal essential medium (Invitrogen, Carlsbad, CA) supplemented with 10% FCII (HyClone, South Logan, UT) and gentamicin/kanamycin (UNC Tissue Culture Facility). Mink lung epithelial cells (Mv1lu) were grown in Dulbecco's minimal essential medium (Invitrogen, Carlsbad, CA) supplemented with 10% FCII (HyClone, South Logan, UT) and gentamicin/kanamycin (UNC Tissue Culture Facility). HAE cells were obtained from airway tissues harvested from patients undergoing elective surgery according to the UNC Institutional Review Board-approved protocols of the UNC

Cystic Fibrosis Center Tissue Culture Core. Briefly, primary cells were expanded on plastic to generate passage 1 cells and plated at a density of 250,000 cells per well on permeable Transwell-Col (12-mm-diameter) supports (8, 33). HAE cell cultures were generated by the provision of an air-liquid interface for 4 to 6 weeks to form well-differentiated, polarized cultures that resemble in vivo pseudostratified mucociliary epithelia (33). All virus work was performed in a class II biological safety cabinet in a certified biosafety level 3 laboratory containing redundant exhaust fans and by laboratorians wearing Tyvek suits and powered air-purifying respirators as described previously (56).

Construction of chimeric SARS-CoVs bearing the SZ16 spike protein icSZ16-S. The infectious clone of the epidemic strain from R. Baric's laboratory is divided into six subgenomic cDNA clones (A to F) that span the SARS-CoV genome. The first two-thirds of the S gene is located within the icSARS E fragment (nucleotides [nt] 21492 to 24056), and the last third is located within the icSARS F fragment (nt 24057 to 25259). A synthetic DNA containing SZ16 nt 21541 to 24056 was purchased from Blue Heron Technology (Bothell, WA). The fragment was digested with AgeI and XbaI (NEB, Ipswich, MA) and cloned into the existing icSARS-E pSMART plasmid, replacing the Urbani S glycoprotein with the SZ16 variant sequence to create icSZ16-E pSMART. Within the SARS F fragment, the two remaining coding changes of the SZ16 S were introduced via PCR and the class II restriction enzyme AarI. Briefly, three amplicons, A, B, and C, were generated by PCR using Expand high-fidelity polymerase (Roche, Indianapolis, IN). The primer pairs used are as follows: amplicon A, PasIF (5′-CTGTTTTCCCTGGGATCGC-3′) and AarIM1NR (5′-NNNNNNCACCTGCTTTTGGGCAACTCCAATGCC-3′); amplicon B, AarIM1NF (5′-NNNNNNCACCTGCAGTTGCCCAAAATGTTCTCTATGAGAAC-3′) and AarIM2NR (5′-NNNNNNCACCTGCATTTCTTCTTGAATGTTGACGACAGAAG-3′); and amplicon C, AarIM2NF (5′-NNNNNNCACCTGCTCAAGAAGAAATTGACCGCCTC-3′) and BamHIR (5′-CATAAATTGGATCCATTGCTGG-3′). Amplicons A, B, and C were digested with AarI for 1.5 h at 37°C (Fermentas, Burlington, Ontario, Canada), gel purified, and ligated to create the fragment ABC. The ABC ligation products were gel purified, and TA was cloned into TOPO-XL (Invitrogen, Carlsbad, CA) to create pTOPO-XL ABC. The pTOPO-XL ABC subclones were confirmed by sequencing. pTOPO-XL ABC was BamHI digested at 37°C for 1 h, which released a 2,059-nt fragment containing the icSZ16 F fragment S sequence. icSARS F-pSMART was digested with BamHI at 37°C for 1 h, which excised the epidemic strain S sequence and released a 5,749-bp vector fragment. The 2,059-bp SZ16 insert and the 5,749-bp vector fragments were gel purified using a QIAquick gel purification kit (Qiagen, Valencia, CA) and ligated (NEB, Ipswich, MA) to create icSZ16 F-pSMART.

Construction of the chimeric icSZ16-S K479N mutant. The icSZ16-E pSMART sequence for S residue 479 was mutated from lysine (AAA) to an asparagine (AAT) using overlap PCR. Amplicon A (NcoIF [5′-TGTTTCTAAACCCATGGGTACACAG-3′] and SZ16479R [5′-CCATAATCATTTAATGGCCAATAAC-3′]) and amplicon B (SZ16479NF [5′-GTTATTGGCCATTAAATGATTATGG-3′] and XbaIR [5′-GGGCCCTCTAGAGATCGAGC-3′]) were generated using Expand high-fidelity polymerase (Roche, Indianapolis, IN). To join the fragments, amplicons A (1,010 bp) and B (1,153 bp) were used as templates in overlapping PCR with primers NcoIF and XbaIR. The final AB amplicon was purified using a Qiagen PCR purification kit (Qiagen, Valencia, CA) and digested with NcoI and XbaI (NEB, Ipswich, MA) for 1 h at 37°C. The digested amplicon (2.2 kb) was gel purified using a QIAquick gel purification kit (Qiagen, Valencia, CA), ligated to the 5.3-kb NcoI/XbaI fragment of icSARS SZ16-E pSMART, and sequence verified.

Isolation of recombinant viruses. From the ligation of appropriate infectious clone fragments, icSZ16-S or icSZ16-S K479N full-length chimeric cDNA was generated, and full-length transcripts were synthesized, mixed with polyadenylated N gene transcripts, and then electroporated into cells as previously described (56). Clarified supernatants from the icSZ16-S or icSZ16-K479N electroporations were passaged onto naive Vero E6 cells to confirm the presence of replicating virus. If a cytopathic effect (CPE) was not detected, viruses were passaged every 48 h onto Vero E6 cells until cytopathology was observed. With icSZ16-S K479N, a mild CPE was observed at passage 3 (p3), and a more robust CPE was seen by p6. The icSZ16-S K479N p3 and p6 viruses were plaque purified in Vero E6 cells. The S, 3a, E, and M genes of the recombinant viruses were sequence verified, and stocks were grown in T75 flasks and stored at −80°C for future use.

RT-PCR to detect the subgenomic leader containing transcripts. Reverse transcriptase (RT)-PCR to detect the subgenomic leader containing transcripts was performed to demonstrate viral replication. RNA from virus-infected cells was isolated using TRIzol reagent (Invitrogen, Carlsbad, CA), according to protocol. One to five micrograms of total RNA was used to generate cDNA by

Superscript II (Invitrogen, Carlsbad, CA), using random hexamer primers (Invitrogen, Carlsbad, CA). cDNA was then used as a template for the PCR using *Taq* polymerase (NEB, Ipswich, MA) with a leader forward primer (CTCTTG TAGATCTGTTCTCTAAACGAAC) and a reverse primer in the M gene (TT ACTGTACTAGCAAAGCAATATTGTCG). The detection of glyceraldehyde-3-phosphate dehydrogenase (GAPDH) (primer GAPDHF [5′-CATGGGGAA GGTGAAGGTCG-3′] and primer GAPDHR [5′-TTGATGGTACATGACAA GGTGC-3′]) messages by RT-PCR was done as a positive control. The PCR products were separated by gel electrophoresis on 1.8% agarose–Tris-acetate-EDTA gels and visualized by ethidium bromide staining.

In vitro evolution of icSARS SZ16 K479N in HAE cell cultures for 22 days. HAE cell cultures were created as described previously (43). The cultures were infected with 10^5 PFU of icSARS K479N in a 200-µl volume. After a 2-h infection, the inoculum was removed, and the cells were washed briefly with Dulbecco's phosphate-buffered saline (DPBS) and then maintained for 4 days. After 4 days of infection, the apical surfaces of the cultures were rinsed, and supernatants were placed onto the apical surfaces of fresh cultures for 1 h, washed, and maintained for another 4 days. Apical washes were then plaque purified to isolate the icSZ16-S K479N D8 virus. A total of 200 µl of day 8 supernatants was used to infect naive HAE cell cultures as described above, and the cultures were passaged two additional times at 4-day intervals and then three times every 48 h to preferentially enrich for more efficiently replicating virus variants. After 22 days of selection for efficient growth in HAE cells, the apical surfaces were rinsed and the supernatants were plaque purified to isolate the icSZ16-S K479N D22 virus. Plaques were expanded on 60-mm dishes, and RNA was isolated using TRIzol (Invitrogen Carlsbad, CA). Amplicons spanning from the S, 3a, E, and M genes were generated by RT-PCR and directly sequenced.

Generation of hACE2-expressing DBT cells. A plasmid carrying an N-terminal myc-tagged human ACE2 (hACE2) was kindly donated by M. Farzan of Harvard Medical School. The hACE2 gene was amplified by PCR using Expand high-fidelity polymerase (Roche, Indianapolis, IN) (ACE2For [5′-CACCATGTCAA GCTCTTCCTGGCTCC-3′] and ACE2Rev [5′-CTAAAAGGAGGTCTGAAC ATCATCAGTG-3′]). Amplicons were gel purified using the QIAquick gel purification kit (Qiagen, Valencia, CA) and cloned into pcDNA3.1/V5-His (Invitrogen, Carlsbad, CA) according to protocol to create pcDNA3.1/V5-His hACE2. The ACE2 gene plasmid was sequence verified. DBT cells were transfected with 4 µg of pcDNA3.1/V5-His hACE2 using Fugene reagent (Roche, Indianapolis, IN). After 24 h, the cells were placed under drug selection using 700 µg/ml of G418 (Invitrogen, Carlsbad, CA) in complete growth medium and remained under drug selection throughout all experiments. The cells were passaged four times, sorted for high ACE2 expression by flow cytometry, and then expanded under drug selection before use.

Growth curve analysis of HAE, Vero E6, DBT hACE2, or DBT cells. HAE cells were infected with 4.4×10^4 PFU of the recombinant epidemic strain icSARS, icSZ16-S K479N p3, icSZ16-S K479N D8, or icSZ16-S K479N D22 for 2 h at 37°C, after which the inoculum was removed and the apical surface rinsed with DPBS. At 0, 6, 12, 24, 36, 48, and 72 h postinfection (hpi), the apical surfaces of the HAE cells were rinsed with 200 µl DPBS and the samples stored at −80°C until titration by plaque assay. Vero E6 and DBT hACE2 cells were infected with icSARS, icSZ16-S K479N p3, icSZ16-S K479N p6, icSZ16-S K479N D8, or icSZ16-S K479N D22 at a multiplicity of infection (MOI) of 0.01 for 1 h at 37°C, after which the inoculum was removed, the monolayer was rinsed with DPBS, and growth medium was added. DBT cells were infected in a similar manner and with the same panel of viruses as the Vero E6 and DBT hACE2 cells, except that icSZ16-S K479N p3 was excluded from the experiment. The cell media were sampled at 0, 6, 12, 24, and 36 hpi, and the samples were stored at −80°C until titers were determined by plaque assay (56). The growth curve data presented are representative of two separate experiments.

Immunohistochemistry of infected HAE cells. To detect SARS-CoV antigens in HAE cells, infected or mock-infected cultures were fixed in 4% paraformaldehyde (PFA) for 24 h, transferred to 70% ethanol, and prepared as paraffin-embedded histological sections by the UNC Cystic Fibrosis Center Morphology and Morphometrics Core. After deparaffinization, histological sections were incubated for 1 h in PBS containing 3% bovine serum albumin. Primary antibodies directed against SARS N or tubulin were applied at a 1:100 dilution in PBS with 1% bovine serum albumin overnight and detected with fluorescein isothiocyanate or Texas Red secondary antibodies (anti-mouse antibodies conjugated to Texas Red; Jackson ImmunoResearch). Immunofluorescence was visualized with a Leica Leitz DMIRB inverted fluorescence microscope equipped with a cooled-color, charge-coupled digital camera (MicroPublisher, Q-Imaging). A tricolor filter cube set (green fluorescent protein-Texas Red-DAPI [4′,6′-diamidino-2-phenylindole]) was used to show the morphology of the tissue section (by combining low autofluorescence levels across the three filters), thus

aiding the determination of fluorescent-antibody localization to specific regions of the cells.

Plaque reduction neutralization titer assay. Neutralizing titers were determined by plaque reduction neutralization titer assay (PRNT) (40). Twenty-four hours prior to infection, six-well plates were seeded with 5×10^5 Vero E6 cells/well. A human monoclonal antibody (MAb), S230.15, directed against the SARS-CoV RBD and an isotype control antibody, D2.2, directed against cholera toxin were kindly provided by A. Lanzavecchia. The MAbs were serially diluted twofold and incubated with 100 PFU of either icSARS, icSZ16-S K479N p6, icSZ16-S K479N D8, or icSZ16-S K479N D22 for 1 h at 37°C. Virus and antibodies were then added to six-well plates of Vero E6 cells in duplicate and incubated at 37°C for 1 h, after which the cells were overlaid with 3 ml of 0.8% agarose in medium. The plates were incubated for 48 h at 37°C and stained with neutral red for 3 h, and the plaques were counted. The percentages of neutralization were calculated as follows: $1 − $ (number of plaques with antibody/number of plaques without antibody) $\times 100\%$.

Infection of 6-week-old and senescent BALB/c mice. Six-week-old female BALB/c mice (Charles River, Wilmington, MA) or 12-month-old female BALB/c mice were anesthetized with a ketamine and xylazine mixture administered intraperitoneally in a 50-µl volume. Each mouse was inoculated with 1×10^5 PFU/50 µl of icSARS, icSZ16-S K479N p6, or icSZ16-S K479N D22 intranasally (10 mice for each virus for the 6-week-old animals; 12 mice for each virus for the 12-month-old animals), and weight was monitored daily for 4 days postinfection. On days 2 and 4, three mice per group were sacrificed by isoflurane overdose, and the lungs were removed for virus titer determination. One-half of each lung was frozen at −80°C until titration by plaque assay. The lungs were weighed and homogenized, and PBS was added to generate a 20% solution. The solution was then clarified by centrifugation and serially diluted for use in a standard plaque assay with Vero E6 cells (56).

Phylogenetic analysis of SARS-CoV spikes and computer modeling. Nucleotide and protein sequence alignments of Urbani (GenBank accession no. AY27841), HKU3 (GenBank accession no. DQ022305), HC/SZ/61/03 (GenBank accession no. AY515512), SZ16 (GenBank accession no. AY304488), GD03 (GenBank accession no. AY525636), GZ02 (GenBank accession no. AY390556), and CUHK-W1 (GenBank accession no. AY278554) were created using ClustalX v1.83 (37). A neighbor joining tree was generated from the ClustalX nucleotide sequence alignment, bootstrapped 1,000 times, and exported into TreeView to create neighbor joining tree graphics (31). The numbers at each node represent the corresponding bootstrap values.

The crystal structure coordinates of the SARS-CoV RBD interacting with the hACE2 receptor (PDB code 2AJF) were used as a template to generate each set of mutations using the Rosetta Design web server (http://rosettadesign.med.unc.edu/) (21). In each case, the SARS-CoV RBD structure was analyzed using the molecular modeling tool MacPyMol (DeLano Scientific) to determine which amino acids were proximal to the amino acid(s) being targeted for replacement. Briefly, each amino acid to be altered was highlighted, and all other amino acids within an interaction distance of 5 angstroms were identified. Using the Rosetta Design website, the amino acid replacements were incorporated, and all amino acids within the 5-angstrom interaction distance were relaxed to allow the program to repack the side chains to an optimal energetic state. This process was repeated for each mutation and series of mutations. Ten models were generated for each set of mutations, and the best model, based on the lowest energy score, was selected and further evaluated using MacPyMol.

RESULTS

Construction and characterization of icSZ16-S and icSZ16-S K479N viruses. Public genetic databases and synthetic biology were harnessed to rapidly translate electronic S gene sequence information into S gene DNA fragments. The SZ16 virus was isolated in live-animal markets in China, and its sequence was published in 2003. When nucleotide sequences of S proteins isolated over the course of the epidemic are compared, the SZ16 S is similar to viruses isolated from Chinese horseshoe bats (HKU3) and to the evolved human-adapted strains (Fig. 1A). The SZ16 S differs from that of the epidemic strain in 18 amino acid positions, 16 of which reside in the S1 region and may well represent the progenitor strains for the 2003 human epi-
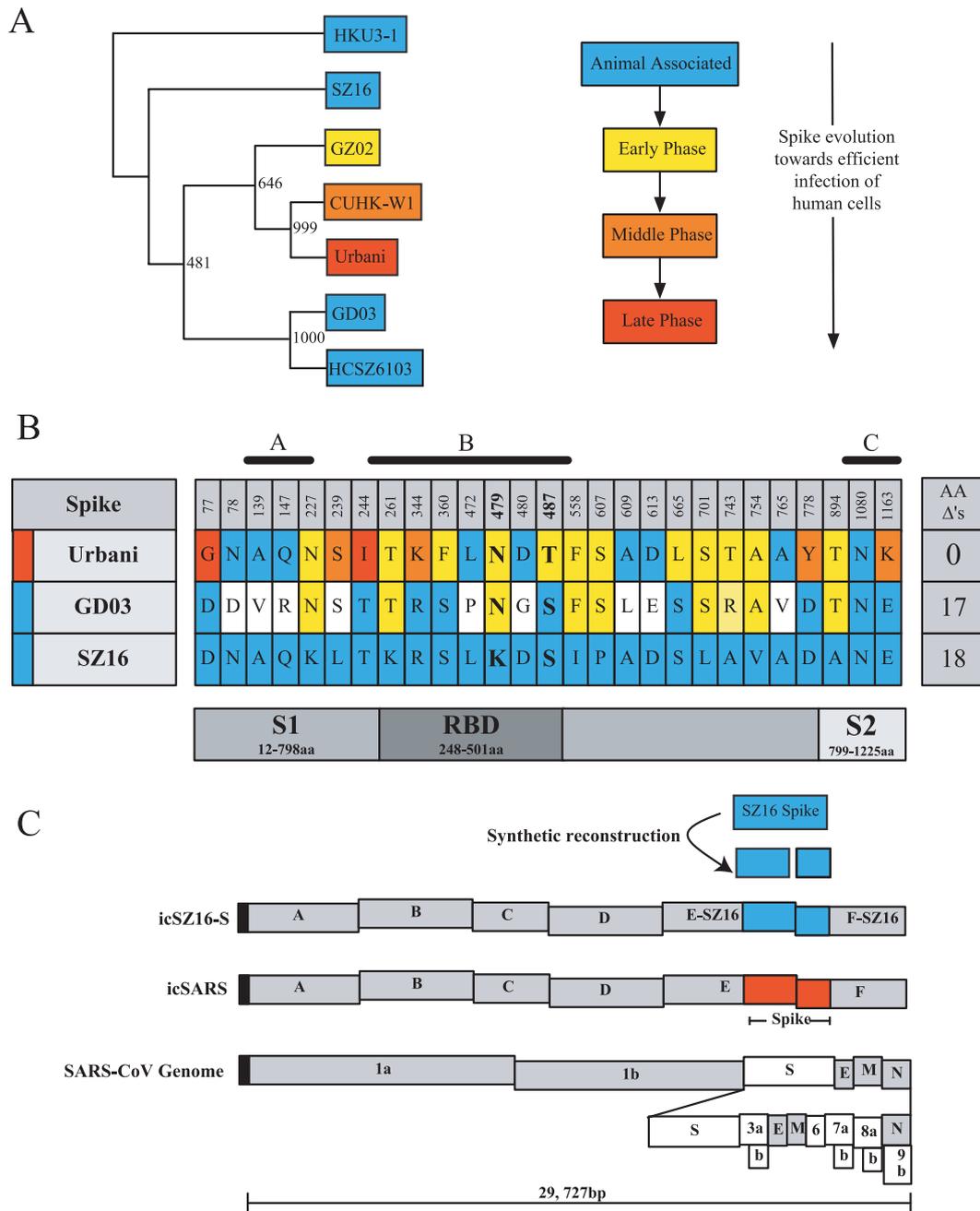
FIG. 1. Phylogenetic relationships of zoonotic SARS-CoV and construction of zoonotic spike protein chimeras within the SARS-CoV infectious clone. The colors in panels A, B, and C denote the phase of the SARS-CoV epidemic at which the viruses or amino acid residues evolved: blue, animal associated; yellow, early phase; orange, middle phase; and red, late phase. (A) Neighbor joining tree constructed from nucleotide sequences of various SARS-CoV S genes. The numbers represent bootstrap values based on 1,000 bootstrap replicates. (B) Spike protein amino acid differences between Urbani, GD03, and SZ16. Known neutralizing epitopes are denoted A, B, and C. (C) Schematic of infectious clone fragments A to F and the SARS-CoV genes contained therein. Using synthetic biology and site-directed mutagenesis, we reconstructed the SZ16 S that was then inserted into our infectious clone, replacing the epidemic strain S.

demic. Much of the SZ16 sequence variability maps in and around the three known neutralizing epitopes marked as regions A, B, and C in Fig. 1B, suggesting that human MAbs derived from human SARS-CoV infections might be less efficacious against SZ16 early civet isolates. As the SZ16 virus could not be successfully maintained in culture, we used synthetic biology and reverse genetics to molecularly

resurrect a recombinant and genetically modifiable SARS-CoV bearing the SZ16 S glycoprotein (icSZ16-S) (Fig. 1C).

Although icSZ16-S recombinant virus infection was not evident by cytopathology-based assays or by plaque assay, RT-PCR confirmed the presence of virus replication within the electroporated cell culture by detecting the subgenomic leaders containing transcripts for open reading frames 3a, E, and M
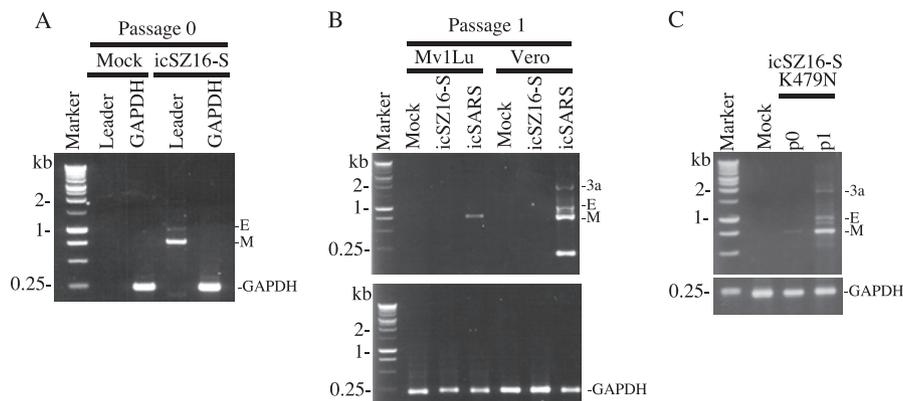
FIG. 2. SARS-CoV SZ16 spike protein chimera icSZ16-S replicates in Vero E6 cells, but infection cannot be passed in culture until a point mutation (K479N) is introduced within the RBD. The expected sizes of the target RT-PCR products are as follows: for 3a, 1,796 bp; E, 949 bp; M, 666 bp; and GAPDH, 235 bp. (A) RT-PCR for the leader containing transcripts detects actively replicating genomic RNA. RT-PCR using RNA extracted from Vero E6 cells transfected with genomic icSZ16-S RNA (passage 0) detects transcripts for the E and M genes of icSZ16-S. (B) The transfer of icSZ16-S supernatants from passage 0 to naive Vero E6 or mink lung epithelial Mv1Lu cells does not result in a productive infection. As a positive control, Vero E6 and Mv1Lu cells were successfully infected with epidemic strain supernatants, as replication was detected by the presence of the leader containing transcripts. (C) In contrast to wild-type icSZ16-S, a point mutation (K479N) in the icSZ16-S spike protein allows for passage of icSZ16-S K479N virus into Vero E6 cells.

(Fig. 2A). The transfer of the icSZ16-S supernatants from the electroporated cell culture to a naive Vero E6 or a mink lung epithelial (Mv1Lu) cell culture did not result in a productive infection, as the leader containing transcripts was not detected (Fig. 2B). As a positive control, we passaged icSARS supernatants to Vero E6 and Mv1Lu cell cultures, and both infections resulted in detectable wild-type virus replication by RT-PCR (Fig. 2B).

Since the icSZ16-S genomic RNA was capable of replicating in Vero E6 cells but the progeny virions were incapable of reinfection and amplification, we hypothesized that the infection was blocked due to inefficient S glycoprotein and ACE2 receptor interaction. In 2005, Li et al. crystallized the RBD of SARS-CoV bound to ACE2 and proposed that residues 479 and 487 of the civet S inhibited efficient usage of the hACE2 receptor (21). Using site-directed mutagenesis, we changed residue 479 of the SZ16 S from lysine to the more human tropic asparagine (K479N) and constructed and recovered the recombinant virus (icSZ16-S K479N). Unlike icSZ16-S virus infection, icSZ16-S K479N infection could be passed on to Vero E6 cell cultures by the transfer of supernatants to naive cell cultures (Fig. 2C), providing direct support for the hypothesis that SZ16 infection of human and/or primate cells is blocked by the civet S residue at position 479.

In vitro evolution of icSZ16-S K479N virus in primary HAE cell cultures. Zoonotic reintroductions represent the most likely mechanism for the reemergence of epidemic SARS-CoV strains in human populations. The SZ16 S K479N mutation permitted binding and entry into primate cells, but our preliminary data suggested that infections of HAE were inefficient (data not shown). To select for civet viruses with enhanced growth in HAE cells, cultures were apically infected with icSZ16-S K479N and maintained and passaged for a total of 22 days. The virus isolated after 8 days in culture, icSZ16-S K479N D8, contained one mutation from tyrosine to phenylalanine at position 442 within the RBD (Y442F). The virus recovered after 22 days in culture, icSZ16-S K479N D22, con-tained the Y442F mutation as well as an additional mutation within the RBD from leucine to phenylalanine at position 472 (L472F). No other coding mutations were found in the S, 3a, E, or M genes. Interestingly, both 442 and 472 are contact residues between S and ACE2 according to the reported crystal structure (21).

The evolved icSZ16-S K479N D8 and D22 viruses exhibit growth kinetics similar to those of the wild type in various cell types. The growth fitness of icSARS, icSZ16-S K479N p3, and the HAE-cell-evolved icSZ16-S K479N D8 and D22 viruses was assessed with HAE cells, Vero E6 cells, murine DBT cells stably expressing hACE2, and nonpermissive murine DBT cells. HAE cell cultures were infected with 4.4×10^4 PFU of virus for 2 h and then rinsed, and apical wash samples were taken at various intervals over 72 hpi to monitor virus growth. The epidemic strain, icSARS, grew to peak titers approaching 10^7 PFU/ml by 72 hpi (Fig. 3A). icSZ16-S K479N p3 grew poorly in the HAE cell cultures, with peak titers reaching only 10^3 PFU/ml (Fig. 3A). Compared to the epidemic strain, the icSZ16-S K479N D22 virus grew with similar growth kinetics at early time points, but peak titers were reduced by about 1 log and approached $\sim10^6$ PFU/ml by 72 hpi (Fig. 3A). The growth of the icSZ16-S K479N D8 virus lagged at early time points but recovered to peak titers similar to that of the icSZ16-S K479N D22 virus (Fig. 3A). In Vero E6 cells, the epidemic strain and the icSZ16-S K479N D22 virus reached peak titers of 10^7 PFU/ml 24 hpi, while icSZ16-S K479N D8, icSZ16-S K479N p3, and icSZ16-S K479N p6 grew to 10^5 PFU/ml (Fig. 3B).

To model the SARS S and hACE interactions within the primary HAE cells and to prove that these mutations were influencing docking and entry via hACE2, we constructed DBT cells that stably express hACE2. In comparison to those of HAE cells, viral growth kinetics were more rapid in DBT-hACE2, although the overall trends in growth among viruses were more or less conserved. In DBT-hACE2 cells, icSARS replicated to peak titers of 10^7 PFU/ml by 24 hpi and then diminished over time to 10^6 PFU/ml by 36 hpi (Fig. 3C).
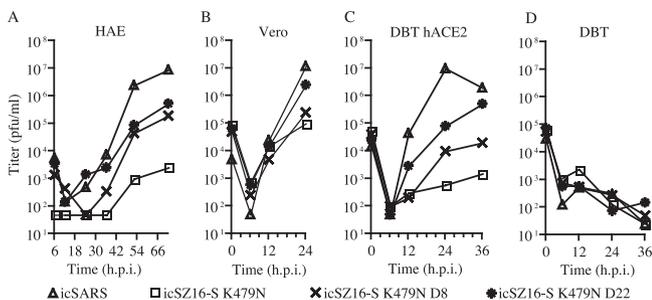
FIG. 3. Growth curve analysis of the mutant virus panel in HAE, Vero E6, DBT-hACE2, and DBT cells. (A) HAE cell cultures were infected with 4.4×10^4 PFU/200 µl of the indicated viruses for 2 h at 37°C. The inoculum was removed, and the apical surfaces were rinsed with DPBS. Apical-surface washes were performed at 0, 6, 12, 24, 36, 48, and 72 hpi. Virus titers were assessed for Vero E6 cells by a standard plaque assay. (B to D) Vero E6, DBT-hACE2, and DBT cells (respectively) were infected with the indicated viruses at an MOI of 0.01 for 1 h at 37°C. The inoculum was removed, cultures were rinsed with DPBS, and growth medium was added. The medium was sampled at 0, 6, 12, 24, and 36 hpi, and virus titer was assessed by plaque assay on Vero E6 cells. The data presented are representative of two separate experiments.

Similarly to the HAE model, early growth of the icSZ16-S K479N D22 virus was more rapid than that of the icSZ16-S K479N D8 virus in DBT-hACE2, but the growth of icSZ16-S K479N D8 virus never matched the icSZ16-S K479N D22 virus growth even after 36 hpi (Fig. 3C). Similarly to the HAE model, the icSZ16-S K479N p3 and the icSZ16-S K479N p6 viruses replicated poorly in DBT-hACE2 cells, reaching titers of only 10^3 PFU/ml by 36 hpi (Fig. 3C). DBT cells did not support the replication of any of the viruses

within our panel, which supports the hypothesis that the expression of ACE2 within DBT-hACE2 cells is required for the growth of all viruses within our panel (Fig. 3D).

Immunohistochemistry of infected HAE cells. Host range expansion of other coronaviruses resulted in a change in cell tropism that was oftentimes associated with a change in receptor usage (4, 27). To determine the types of cells infected by the panel viruses in HAE, infected cultures were fixed and sectioned for the histological staining of SARS-CoV nucleocapsid antigen and tubulin for the staining of cilia. SARS N antigen was not detected in mock-infected cultures, though cilia on the apical surface of ciliated epithelial cells show bright staining (Fig. 4A). SARS N antigen is readily detected within the ACE2-expressing ciliated cells of icSARS (Fig. 4B)- and icSZ16-S K479N D22 (Fig. 4D)-infected cell cultures but is only sporadically detected in icSZ16-S K479N p6 (Fig. 4C)-infected cell cultures. Nevertheless, the HAE-evolved icSZ16-S K479N D22 virus and the parent zoonotic icSZ16-D K479N virus encode ciliated cell tropisms that are similar to those seen in late-phase epidemic strains.

PRNT using human MAb S230.15. Future outbreaks of SARS-CoV would most likely emerge from pools of zoonotic virus, and it is imperative that vaccinations or serotherapies be effective against both past and future emergent zoonotic strains. S230.15 is a human MAb that is broadly neutralizing through its binding to the RBD, though the specific location of the epitope is unknown (48, 59). The epidemic strain and the evolved icSZ16-S K479N D8 and icSZ16-S K479N D22 viruses are equally neutralized by S230.15 (50% neutralization at a concentration between 0.0625 and 0.125 µg/ml), but icSZ16-S K479N is eight times more resistant (50% neutralization at 0.5 µg/ml) (Fig. 5). Since icSZ16-S K479N and the evolved
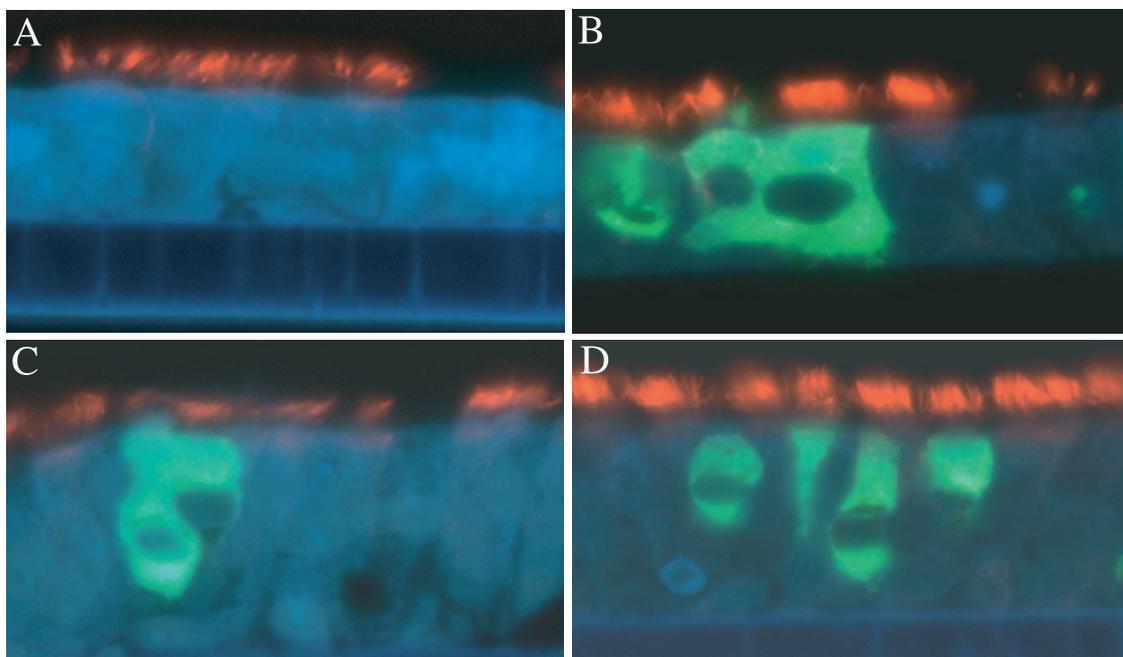

FIG. 4. Immunofluorescence staining of HAE cell cultures infected with the mutant virus panel. At 72 hpi, mock and infected HAE cell cultures were PFA fixed and paraffin embedded for tissue sectioning. Sections were stained for SARS-CoV N (fluorescein isothiocyanate) and tubulin within cilia (Texas Red) and viewed by fluorescence microscopy. (A) Mock; (B) icSARS; (C) icSZ16-S K479N; (D) icSZ16-S K479N D22.
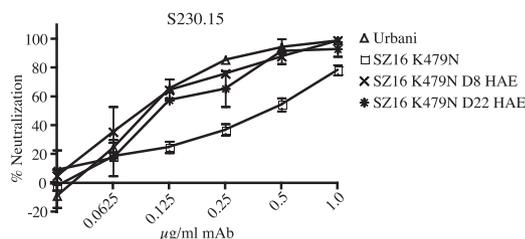
FIG. 5. PRNT assay of the mutant panel viruses using human MAb S230.15. One hundred PFU of the indicated virus was incubated at 37°C for 1 h with twofold dilutions of antibody or DPBS in duplicate. After the incubation, the virus-antibody cocktails were used to infect Vero E6 cell monolayers for 1 h, after which cultures were overlaid with growth medium containing agarose. After 48 h, plaques were enumerated. The percentages of neutralization were calculated as follows: $1 - $ (number of plaques with antibody/number of plaques without antibody) $\times 100\%$. Error bars represent the standard errors of the means.

icSZ16-S K479N D8 virus only differ in 1 amino acid within the S protein, these data suggest that the S230.15 epitope resides near residue 442. Moreover, these data suggest that as SZ16-like zoonotic SARS-CoVs adapt to the hACE2 receptor in the human airway, they may become more susceptible to S230.15 neutralization, especially if they evolve with mutations at residue 442. As an isotype control, an irrelevant cholera-toxin-specific antibody (D2.2) was used in a PRNT assay with the mutant virus panel, and none of the viruses were neutralized at any concentration of the antibody (data not shown).

The icSZ16-S K479N and icSZ16-S K479N D22 viruses replicate in the lungs of young BALB/c mice but do not cause clinical signs in young or senescent BALB/c mice. Since the epidemic strain may not exist in nature and future epidemic SARS-CoV strains would most likely evolve from zoonotic pools of virus, it is prudent to employ an antigenically divergent panel of zoonotic challenge viruses to assess their therapeutic efficacies and cross-reactivities. To this end, it is imperative that the challenge viruses behave similarly in current animal models used to assess vaccine efficacy. Infection of young BALB/c mice with SARS Urbani typically does not cause clinical symptoms (5, 39). Young mice that were either mock infected or infected with the icSARS, icK479N-S K479N, or icSZ16-S K479N D22 viruses did not lose weight or present with other clinical signs (Fig. 6A). Clinical outcomes in senescent mice infected with icSZ16-S K479N or icSZ16-S K479N D22 mirrored those of young mice, with senescent mice losing little to no weight following infection (data not shown). The icSZ16-S K479N and icSZ16-S K479N D22 viruses replicated in the lungs of young BALB/c mice to titers similar to the epidemic strain on day 2 postinfection ($\sim 3 \times 10^6$ PFU/g) (Fig. 6B). By day 4 postinfection, the titers of the civet viruses were about 1 log lower than the epidemic strain, suggesting that the civet viruses might be cleared more rapidly (Fig. 6B).

Rosetta Design modeling of S RBD and ACE2 interactions. Rosetta Design was used to model hACE2's interactions with the RBDs of the SZ16, SZ16 K479N, icSZ16-S K479N D8, and icSZ16-S K479N D22 viruses. In contrast to the epidemic strain N479 residue, the SZ16 K479 residue appears to electrostatically clash with the ACE2 binding partners K31 and H34. After a point mutation (K479N) is introduced in the civet
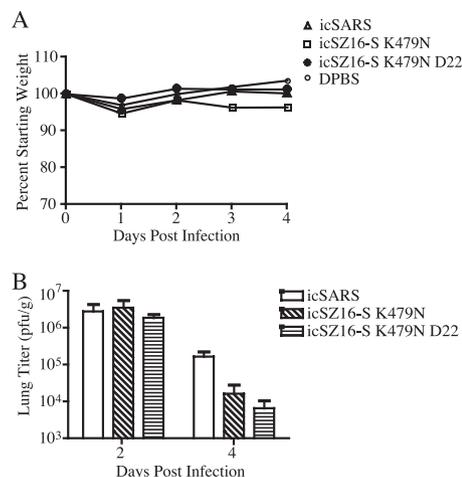

FIG. 6. Clinical signs and lung virus titers of 6-week-old BALB/c mice infected with DPBS, icSARS, icSZ16-S K479N, or icSZ16-S K479N D22. (A) Mice were infected with 10^5 PFU/50 μl intranasally (10 mice per virus), and weight was monitored daily. (B) Lungs were removed on days 2 and 4 postinfection (3 mice per group per day), homogenized, and centrifuged to pellet debris. Supernatants were used in a standard plaque assay to determine lung virus titers (PFU/g).

S RBD, the repulsive forces of the civet K479 are eradicated, allowing for S and ACE2 binding (Fig. 7A, B, and C). The Urbani RBD residues 442 and 479 are predicted to have single hACE2 binding partners (residue 442 interacts with H34; residue 479 interacts with K31) (Fig. 7A). Though residues 442 and 479 of the SZ16 K479N RBD are identical to Urbani, residues 442 and 479 are predicted to compete for hACE2 binding partner H34, and residue 442 is also predicted to interact with H34 and K31 of hACE2 (Fig. 7C). The difference in binding efficiencies of the seemingly similar Urbani and K479N RBDs is likely due to subtle alterations of the RBD hydrogen bonding network created by mutations at the peripheral RBD residue 487. Residue S487 of the SZ16 K479N RBD binds to one ACE2 residue, but T487 of Urbani binds to three residues of ACE2, thereby enhancing S and ACE2 binding interactions (Fig. 7C). The Rosetta Design model predicts that the Y442F mutation within the icSZ16-S K479N D8 S protein creates an RBD architecture similar to that of SARS Urbani, where S residues F442 and N479 have singular and unique hACE2 binding partners (residue 442 binds K31 of hACE2, and residue 479 binds H34 of hACE2) while retaining the S487 and Y41 interaction and the hydrogen bonding network (Fig. 7C and D). Finally, while the icSZ16-S K479N D8 L472 residue is predicted to have only two potential ACE2 binding partners (L79 and M82), the L472F mutation of the icSZ16-S K479N D22 S protein is predicted to increase the numbers of possible binding partners of ACE2 to three residues (L79, M82, and Y83), thereby strengthening S binding (Fig. 7D and E).

DISCUSSION

The past and present sporadic reemergences of the Chikungunya, Ebola, and Nipah viruses highlight the severe pathogenic and epidemic potential of zoonotic viruses, and the identification of the animal reservoir host is often elusive (13, 20, 25, 47, 51). Live-animal markets in China and elsewhere have
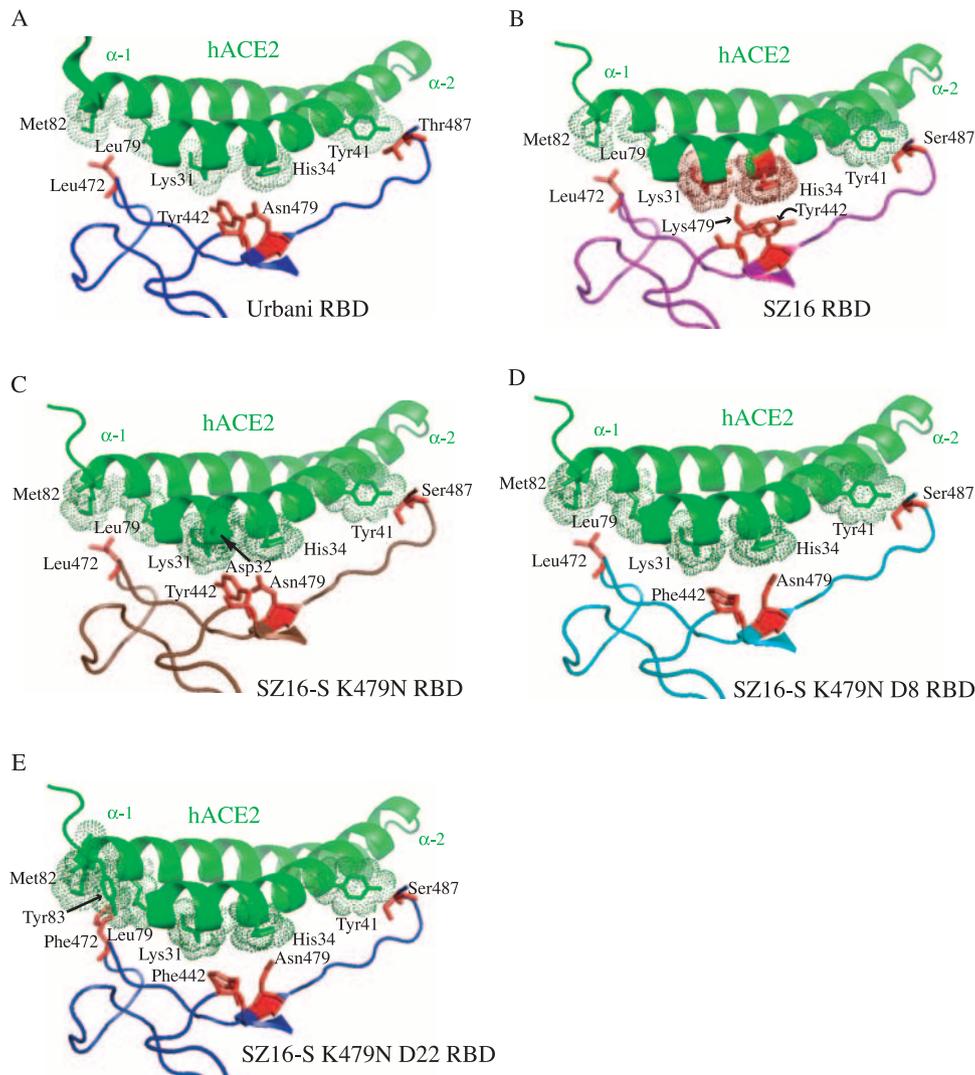
FIG. 7. Rosetta Design modeling of "evolved" mutations that enhance spike protein binding to ACE2. Rosetta Design was used to generate structural models of SZ16 and mutant RBDs that were then superimposed onto the existing crystal structure of the SARS Urbani RBD bound to ACE2. (A) Epidemic strain and hACE2 RBD architecture. (B) SZ16 and hACE2 interaction is inhibited by steric clashing, shown as red dots, of K479 of S and residues K31 and H34 of hACE2. (C) Electrostatic repulsion at residue 479 is eradicated, allowing S and ACE2 binding, but local remodeling within the RBD due to hydrogen bonding differences at residue 487 creates cross-reactions whereby residues 442 and 479 of K479N compete with each other for interaction partners H34, K31, and D32 of hACE2. (D) The Y442F mutation of icSZ16-S K479N D8 restores an optimal RBD, allowing for favorable packing to create an architecture similar to that of the wild type. (E) Leucine 472 of the icSZ16-S K479N and icSZ16-S K479N D8 S interacts with L79 and M82 of ACE2. The icSZ16-S K479N D22 L472F mutation is predicted to have hydrophobic interactions with three potential partners, L79, M82, and Y83, of hACE2 that will increase the stability of the binding. Green dots on hACE2 indicate residues which are within 4 angstroms and thus are predicted to interact with the S residues shown in red.

been proven to be an important factor in cultivating food-borne illnesses and cross-species transmission of SARS-CoV, avian influenza viruses, and other pathogens (29, 54, 55). Within the live-animal markets of China, dense human and animal populations mix, creating an environment ripe for the exchange of viruses from animals to humans and from humans to animals. During the SARS-CoV epidemic, the Himalayan palm civet was identified as the principal source of the SARS-CoV zoonosis even though 1,107 civets on farms that supplied the markets tested negative, suggesting that the civets were infected within the markets (16). Moreover, sequence analysis of bat- and civet-associated SARS-CoV has provided more definitive evidence that bat-associated SARS-CoV jumped the

species barrier to infect civets and that bat and civet viruses are similar yet distinct from late-phase epidemic strain isolates (2, 9, 18, 26, 34, 41).

After the identification of ACE2 as the cellular receptor for SARS-CoV, several investigators have defined the molecular determinants of the virus and receptor interactions that allowed for the epidemic SARS-CoV host expansion. Prior to this report, key residues in the civet S gene responsible for changes in the host range were identified using SARS-CoV S pseudotyped retroviruses, but these results had not yet been confirmed in the context of wild-type SARS-CoV infection in vivo or in vitro. In support of data from Li et al., we demonstrate that the civet-spiked icSZ16-S virus was capable of a

single round of replication following transfection of full-length genomic RNA but was incapable of infecting naive Vero E6 cells in subsequent rounds of infection (21). However, the introduction of a single amino acid mutation (K479N) in the icSZ16-S virus S protein allowed for low-level spread and passage in Vero E6 cells. Both icSZ16-S K479N p3 and p6 viruses grew similarly in Vero and DBT-hACE2 cells, suggesting that the slight differences in their abilities to cause CPE did not affect virus binding, entry, or replication fitness during the time observed and at the MOI used in our assays. Though we did not use icSZ16-S K479N p6 in our HAE cell growth studies, we would expect both p3 and p6 isolates to perform similarly, since their growth kinetics in Vero and DBT-hACE2 cells were similar. Importantly, the K479N mutation did not result in a virus capable of efficient replication in HAE or DBT-hACE2 cells, supporting the argument that additional mutations are required to enhance the SZ16 S interaction with the human ACE2 receptor. The differences seen in icSZ16-S K479N growth in HAE and Vero E6 cells highlight the strength and relevance of the HAE model of the human airway. Even though the contact residues of primate and human ACE2 are predicted to be similar, the differences in icSZ16-S K479N growth in HAE and Vero E6 cells suggest that differences in primate and human ACE2 proteins (89% similar on the amino acid level) subtly influence binding efficiency or that the abundance of mucus and a unique extracellular matrix on the surfaces of HAE cells differentially antagonize virus entry. Thus, in order to study and model S protein and hACE2 interactions, HAE or DBT-hACE2 cells should be used as more relevant alternatives to Vero E6 cells. Importantly, the expression of hACE2 in a nonpermissive DBT cell line rendered these cells permissive for icSARS, icSZ16-S K479N, icSZ16-S K479N D8, and icSZ16-S K479N D22 virus infection, which strongly supports earlier hypotheses that ACE2 is the principal receptor required for the docking and entry of both human and zoonotic strains (24).

For both the canine parvovirus (CPV) and the 1918 Spanish influenza virus H1N1, point mutations in the viral structural proteins responsible for binding to the host cell were sufficient to catalyze host range expansion (14, 46). In 1978, two mutations in the capsid protein of feline parvovirus that were sufficient to catalyze host expansion evolved, causing severe canine infection and a worldwide epidemic of CPV-naive canine populations (14, 32). In 1918, the zoonotic H1N1 influenza virus acquired two mutations in hemagglutinin, changing the preferential binding from the avian to the human sialic acid receptor. When the hemagglutinin mutations were coupled with a few additional mutations in the genome, a human pandemic ensued with estimated deaths of 20 million to 40 million (32, 46). Similarly to those of the CPV and H1N1 viruses, analyses of the zoonotic and human SARS-CoV S sequences show a logical progression of S protein mutations that most likely fostered host range expansion and increased human pathogenesis (16). Of the 14 amino acids of S that contact 18 amino acids of ACE2, the K479N and S487T mutations have been shown to be equally essential for civet S adaptation to human ACE2 (21). The K479N mutation removed an electrostatic clash, allowing the S protein RBD to interact with human ACE2, while S487T appears to have subtly remodeled the RBD through hydrogen bonding differences that optimized

hACE2 binding. Considering our in vitro evolution data and sequence data from the SARS epidemic, we hypothesize that at least two independent mutational pathways can optimize hACE2 binding. The first was observed during the epidemic, where the S487T mutation optimized binding as described above. The second route occurred during our in vitro evolution, whereby the Y442F mutation optimized hACE2 binding in the presence of the S487 variant. ACE2-expressing ciliated epithelial cells in the airway are targets for SARS-CoV infection in humans, primate and rodent models making the HAE model an important in vitro system for studying the molecular mechanisms of animal S adaptation to the human host (10, 11, 30, 38, 39). Since the icSZ16-S virus could not be propagated in Vero E6 cells, we introduced the K479N point mutation in the virus S that was sufficient to allow multiple rounds of replication of the civet-spiked icSZ16-S K479N virus in cell culture. Passage of the icSZ16-S K479N recombinant virus in HAE cells resulted in the emergence of S variants that could replicate more efficiently. Surprisingly, S487T was not selected with the passage of SZ16 K479N, but new mutations evolved within contact residues of the icSZ16-S K479N D8 and icSZ16-S K479N D22 virus RBDs (Y442F and L472F) that enhanced virus infection of HAE, Vero E6, and DBT-hACE2 cells. To rule out non-receptor-specific cell culture adaptations that enhance entry into cells in vitro, we infected DBT cells and did not see evidence of virus growth with any of the viruses tested. Moreover, our immunohistochemistry of infected HAE cell cultures (Fig. 4) suggests that in vitro-evolved viruses and the epidemic strain infect similar cell types, providing further support that non-receptor-specific entry adaptations had not occurred in our model. Recent passage of a related coronavirus, mouse hepatitis virus, in cell lines resulted in variants with an expanded host range due to the acquisition of a common non-receptor-specific cell culture adaptation using heparin sulfate for virus entry into cells (4). Most recently, McRoy and Baric demonstrated that the passage of mouse hepatitis virus in cell lines resulted in an expanded host range through mutations within the fusion peptide and heptad repeats, demonstrating that host range can be governed by changes in spike fusogenicity (27). From sequence analysis, we concluded that the in vitro evolved mutations of icSZ16-S K479N had not created a heparin consensus binding site (XBXBBX) and that our adaptive mutations were constrained to the RBD.

To determine the potential impact of the mutations acquired during HAE passage, we used Rosetta Design to generate structural models of the SZ16, icSZ16-S K479N, icSZ16-S K479N D8, and icSZ16-S K479N D22 RBDs and then superimposed these models onto the existing crystal structure of the SARS Urbani RBD bound to hACE2 (PDB code 2AJF) (Fig. 7A). Similarly to Li et al., we observed that residue K479 of the SZ16 S inhibited binding to hACE2 by sterically clashing with residues K31 and H34 (Fig. 7B). After the K479N mutation, the electrostatic repulsion at residue 479 is eradicated, but Rosetta Design predicts that local remodeling within the RBD creates cross-reactions whereby residues 442 and 479 of the K479N RBD compete with each other for interaction with partners H34, K31, and D32 of ACE2 (Fig. 7C). It appears that Y442 could interact with all three hACE2 residues, but N479 is predicted to interact only with H34 of hACE2. We predict that this network of competing interactions reduces the avidity be-

tween the K479N RBD and the hACE2 receptor by misaligning other key residues in the RBD. Of note, the only difference in the RBDs of SZ16 K47N and Urbani occurs at position 487. The fact that SZ16 K479N is compromised in growth compared to Urbani suggests that the hydrogen bonding differences between S487 of SZ16 K47N and Thr487 of Urbani influence the receptor interaction. During the 2003 epidemic, S487T likely evolved to eliminate this putative inhibitory effect. Interestingly, the icSZ16-S K479N D8 Y442F mutation also restores an optimal RBD by allowing for favorable amino acid packing that recreated an RBD architecture similar to that of the wild type (Fig. 7A and D). In this case, the icSZ16-S K479N D8 RBD residues 442 and 479 have distinct and unique interaction partners in hACE2, which likely restores avidity to near wild-type levels and may explain why the icSZ16-S K479N D8 virus grows more efficiently than the icSZ16-S K479N virus in cells expressing hACE2 (Fig. 3C and 7D). Thus, at least two independent routes of evolution could increase S RBD and human ACE2 interactions. Leucine 472 of the icSZ16-S K479N RBD and the icSZ16-S K479N D8 RBD interacts with L79 and M82 of ACE2. The icSZ16-S K479N D22 virus RBD is mutated at position 472 from leucine to phenylalanine, which Rosetta Design predicts will induce strong hydrophobic interactions between F472 and partners L79, M82, and Y83 of ACE2 (Fig. 7E). The icSZ16-S K479N D22 virus F472 mutation likely strengthens the binding interface of the icSZ16-S K479N D22 virus over the icSZ16-S K479N D8 strain, which may explain why the icSZ16-S K479N D22 virus has a growth advantage over the icSZ16-S K479N D8 virus in HAE, Vero E6, and DBT-hACE2 cells. Of note, it is possible that these viruses acquired replication-enhancing mutations in structural or nonstructural genes that we did not sequence. Nevertheless, these data demonstrate the plasticity of the RBD-ACE2 interface site and its ability to subtly remodel the RBD and hACE2 binding interface to promote efficient entry and growth. Clearly, multiple genetic pathways likely exist to allow for zoonotic SARS-CoV host range expansion, and it will be interesting to determine if other contact interface point mutations can enhance zoonotic virus infection of HAE cell cultures.

Since viruses similar to the epidemic strain are currently circulating in bats in China, we may see yet another emergence of human SARS-CoV from zoonotic pools of virus. Therefore, it is imperative that current vaccinations and passive serotherapies be effective against all known SARS-CoV zoonotic strains and their human-adapted progeny. Previous work by Deming et al. has highlighted the value of using zoonotic strains as challenge viruses to assess vaccine efficacy (5). Deming et al. demonstrated that sera from animals vaccinated with epidemic strain antigens were not as effective in neutralizing the zoonotic icGD03-S virus as they were in neutralizing the epidemic strain (5). Within this study, we demonstrated that two zoonotic spiked viruses, icSZ16-S K479N and icSZ16-K479N D22, grew to peak titers in the mouse lung similar to those of the epidemic strain 2 days postinfection. In contrast to recombinant SARS-CoV bearing early human (GZ02) or civet S glycoprotein (HC/SZ/61/05) S proteins that were extremely pathogenic in aged animals, icSZ16-S K479N and icSZ16-S K479N D22 caused little to no disease in either young or senescent BALB/c mice (40). Although the SZ16 and HC/SZ/

61/03 viruses are both of civet origin, their S proteins differ by 18 amino acids (9; G. Yi, SARS coronavirus HC/SZ/61/03 complete genome). The 7-month period of time between the isolation of SZ16 (May 2003) and the isolation of HC/SZ/61/03 (December 2003) may help explain their sequence differences (9; G. Yi, SARS coronavirus HC/SZ/61/03 complete genome [http://www.ncbi.nlm.nih.gov/entrez/viewer.fcgi?db=nuccore&id=42556132]). Zoonotic SARS-CoV infection of humans is typically less severe than infection with human strains, but it is possible that the sequence differences between the SZ16 and the HC/SZ/61/03 S proteins alter the structure of the S proteins such that the viruses bearing the HC/SZ/61/03 S are lethal in mice, while our SZ16 lineage viruses are attenuated (2, 9, 19, 23, 40, 45). Nevertheless, the icSZ16-S K479N and icSZ16-S K479N D22 viruses grow to levels similar to those of the epidemic strain in mice and could be useful as challenge viruses to assess the efficacies of vaccines or serotherapies. The human MAb S230.15 binds within the RBD, although the specific epitope has yet to be defined (48, 59). Recent data from Traggiai et al. and Zhu et al. have shown MAbs S230.15 and, to a lesser extent, m396 to be potent and cross-neutralizing antibodies against human and zoonotic SARS-CoV isolates (48, 59). We have demonstrated that the "evolved" icSZ16-S K479N D8 and D22 viruses were equally susceptible to neutralization by S230.15 but that icSZ16-S K479N was eight times more resistant. In this instance, these data suggest that zoonotic virus adaptation to the human ACE2 receptor may enhance susceptibility to neutralization by S230.15. Since there was a dramatic difference in neutralization between icSZ16-S K479N and icSZ16-S K479N D8, these data suggested that the epitope of S230.15 is in close proximity to or was affected by structural changes associated with residue 442 of the S protein. Future efforts to revive the divergent wild-type icSZ16-S virus in vitro will be especially helpful with mapping the S230.15 epitope, since it is possible that the K479N mutation may contribute to enhanced S230.15 binding. Even though S230.15 is less effective at neutralizing icSZ16-S K479N in vitro, recently published passive transfer studies in mice have shown that the S230.15 antibody is extremely potent and broadly neutralizing in vivo where replication of SARS Urbani, icGD03-S, and icSZ16-S K479N were not detected in the mouse lung (59). These data highlight the power and utility of zoonotic strains in assessing the efficacy of passive serotherapy both in vitro and in vivo.

In conclusion, synthetic biology has been employed to rapidly construct and assemble a completely synthetic and infectious 5.3-kb bacteriophage, poliovirus, 1918 influenza virus, and a panel of SARS viruses bearing animal and human S glycoproteins (1, 5, 40, 44, 49). We provide yet another example of the utility of synthetic biology by resurrecting the civet SZ16 S. We have shown that a single point mutation (K479N) in the SZ16 S facilitates host range expansion, but additional mutations must occur for robust infection of human cells. Mutations of residues 479 (K479N) and 487 (S487T) occurred during the early phase of the SARS-CoV epidemic to help facilitate host range expansion. Though we did not generate a mutant SZ16 S containing S487T, previous studies have shown that the inclusion of a mutation at either position 479 or 487 in pseudotype virus bearing the civet S allowed for the infection of human cells, but this approach provides little information on

growth efficiency and spread. Through our in vitro evolution of the icSZ16-S K479N virus, we discovered a novel evolutionary path by which SARS-CoV S can interface with hACE2 to allow for the efficient infection of human cells. When S mutations acquired during our in vitro evolution are compared to mutations that occurred during the evolution of the epidemic strain, the plasticity of the SARS-CoV S protein becomes starkly apparent. Through the use of HAE cell cultures, synthetic biology, reverse genetics, and animal models, we have created a system to isolate and characterize novel genetic pathways of zoonotic SARS-CoV S adaptation to the human ACE2 receptor. We have also generated antigenically divergent SARS-CoV zoonotic strains that might be useful in assessing the efficacies of SARS-CoV vaccines or serotherapies. Since the future emergence of SARS-CoV will most likely evolve from zoonotic pools of virus, it is imperative that current vaccinations and passive serotherapies be effective against the zoonotic virus, the epidemic virus strain, and all of the evolutionary permutations in between.

REFERENCES

1. Cello, J., A. V. Paul, and E. Wimmer. 2002. Chemical synthesis of poliovirus cDNA: generation of infectious virus in the absence of natural template. Science 297:1016–1018.
2. Chinese SARS Molecular Epidemiology Consortium. 2004. Molecular evolution of the SARS coronavirus during the course of the SARS epidemic in China. Science 303:1666–1669.
3. Christian, M. D., S. M. Poutanen, M. R. Loutfy, M. P. Muller, and D. E. Low. 2004. Severe acute respiratory syndrome. Clin. Infect. Dis. 38:1420–1427.
4. de Haan, C. A. M., Z. Li, E. te Lintelo, B. J. Bosch, B. J. Haijema, and P. J. M. Rottier. 2005. Murine coronavirus with an extended host range uses heparan sulfate as an entry receptor. J. Virol. 79:14451–14456.
5. Deming, D., T. Sheahan, M. Heise, B. Yount, N. Davis, A. Sims, M. Suthar, J. Harkema, A. Whitmore, R. Pickles, A. West, E. Donaldson, K. Curtis, R. Johnston, and R. Baric. 2006. Vaccine efficacy in senescent mice challenged with recombinant SARS-CoV bearing epidemic and zoonotic spike variants. PLoS Med. 3:e525.
6. Domingo, E., and J. J. Holland. 1997. RNA virus mutations and fitness for survival. Annu. Rev. Microbiol. 51:151–178.
7. Drosten, C., S. Gunther, W. Preiser, S. van der Werf, H. R. Brodt, S. Becker, H. Rabenau, M. Panning, L. Kolesnikova, R. A. Fouchier, A. Berger, A. M. Burguiere, J. Cinatl, M. Eickmann, N. Escriou, K. Grywna, S. Kramme, J. C. Manuguerra, S. Muller, V. Rickerts, M. Sturmer, S. Vieth, H. D. Klenk, A. D. Osterhaus, H. Schmitz, and H. W. Doerr. 2003. Identification of a novel coronavirus in patients with severe acute respiratory syndrome. N. Engl. J. Med. 348:1967–1976.
8. Fulcher, M. L., S. Gabriel, K. A. Burns, J. R. Yankaskas, and S. H. Randell. 2005. Well-differentiated human airway epithelial cell cultures. Methods Mol. Med. 107:183–206.
9. Guan, Y., B. J. Zheng, Y. Q. He, X. L. Liu, Z. X. Zhuang, C. L. Cheung, S. W. Luo, P. H. Li, L. J. Zhang, Y. J. Guan, K. M. Butt, K. L. Wong, K. W. Chan, W. Lim, K. F. Shortridge, K. Y. Yuen, J. S. Peiris, and L. L. Poon. 2003. Isolation and characterization of viruses related to the SARS coronavirus from animals in southern China. Science 302:276–278.
10. Haagmans, B. L., T. Kuiken, B. E. Martina, R. A. Fouchier, G. F. Rimmelzwaan, G. van Amerongen, D. van Riel, T. de Jong, S. Itamura, K. H. Chan, M. Tashiro, and A. D. Osterhaus. 2004. Pegylated interferon-alpha protects type 1 pneumocytes against SARS coronavirus infection in macaques. Nat. Med. 10:290–293.
11. Haagmans, B. L., and A. D. Osterhaus. 2006. Nonhuman primate models for SARS. PLoS Med. 3:e194.
12. Hamming, I., W. Timens, M. L. Bulthuis, A. T. Lely, G. J. Navis, and H. van Goor. 2004. Tissue distribution of ACE2 protein, the functional receptor for SARS coronavirus. A first step in understanding SARS pathogenesis. J. Pathol. 203:631–637.
13. Hsu, V. P., M. J. Hossain, U. D. Parashar, M. M. Ali, T. G. Ksiazek, I. Kuzmin, M. Niezgoda, C. Rupprecht, J. Bresee, and R. F. Breiman. 2004. Nipah virus encephalitis reemergence, Bangladesh. Emerg. Infect. Dis. 10:2082–2087.
14. Hueffer, K., J. S. L. Parker, W. S. Weichert, R. E. Geisel, J.-Y. Sgro, and C. R. Parrish. 2003. The natural host range shift and subsequent evolution of canine parvovirus resulted from virus-specific binding to the canine transferrin receptor. J. Virol. 77:1718–1726.
15. Jeffers, S. A., S. M. Tusell, L. Gillim-Ross, E. M. Hemmila, J. E. Achenbach, G. J. Babcock, W. D. Thomas, Jr., L. B. Thackray, M. D. Young, R. J. Mason, D. M. Ambrosino, D. E. Wentworth, J. C. Demartini, and K. V. Holmes. 2004. CD209L (L-SIGN) is a receptor for severe acute respiratory syndrome coronavirus. Proc. Natl. Acad. Sci. USA 101:15748–15753.
16. Kan, B., M. Wang, H. Jing, H. Xu, X. Jiang, M. Yan, W. Liang, H. Zheng, K. Wan, Q. Liu, B. Cui, Y. Xu, E. Zhang, H. Wang, J. Ye, G. Li, M. Li, Z. Cui, X. Qi, K. Chen, L. Du, K. Gao, Y.-T. Zhao, X.-Z. Zou, Y.-J. Feng, Y.-F. Gao, R. Hai, D. Yu, Y. Guan, and J. Xu. 2005. Molecular evolution analysis and geographic investigation of severe acute respiratory syndrome coronavirus-like virus in palm civets at an animal market and on farms. J. Virol. 79:11892–11900.
17. Ksiazek, T. G., D. Erdman, C. S. Goldsmith, S. R. Zaki, T. Peret, S. Emery, S. Tong, C. Urbani, J. A. Comer, W. Lim, P. E. Rollin, S. F. Dowell, A. E. Ling, C. D. Humphrey, W. J. Shieh, J. Guarner, C. D. Paddock, P. Rota, B. Fields, J. DeRisi, J. Y. Yang, N. Cox, J. M. Hughes, J. W. LeDuc, W. J. Bellini, and L. J. Anderson. 2003. A novel coronavirus associated with severe acute respiratory syndrome. N. Engl. J. Med. 348:1953–1966.
18. Lau, S. K., P. C. Woo, K. S. Li, Y. Huang, H. W. Tsoi, B. H. Wong, S. S. Wong, S. Y. Leung, K. H. Chan, and K. Y. Yuen. 2005. Severe acute respiratory syndrome coronavirus-like virus in Chinese horseshoe bats. Proc. Natl. Acad. Sci. USA 102:14040–14045.
19. Lau, Y. L., and J. S. Peiris. 2005. Pathogenesis of severe acute respiratory syndrome. Curr. Opin. Immunol. 17:404–410.
20. Leroy, E. M., B. Kumulungui, X. Pourrut, P. Rouquet, A. Hassanin, P. Yaba, A. Delicat, J. T. Paweska, J. P. Gonzalez, and R. Swanepoel. 2005. Fruit bats as reservoirs of Ebola virus. Nature 438:575–576.
21. Li, F., W. Li, M. Farzan, and S. C. Harrison. 2005. Structure of SARS coronavirus spike receptor-binding domain complexed with receptor. Science 309:1864–1868.
22. Li, W., M. J. Moore, N. Vasilieva, J. Sui, S. K. Wong, M. A. Berne, M. Somasundaran, J. L. Sullivan, K. Luzuriaga, T. C. Greenough, H. Choe, and M. Farzan. 2003. Angiotensin-converting enzyme 2 is a functional receptor for the SARS coronavirus. Nature 426:450–454.
23. Li, W., S.-K. Wong, F. Li, J. H. Kuhn, I.-C. Huang, H. Choe, and M. Farzan. 2006. Animal origins of the severe acute respiratory syndrome coronavirus: insight from ACE2–S-protein interactions. J. Virol. 80:4211–4219.
24. Li, W., C. Zhang, J. Sui, J. H. Kuhn, M. J. Moore, S. Luo, S. K. Wong, I. C. Huang, K. Xu, N. Vasilieva, A. Murakami, Y. He, W. A. Marasco, Y. Guan, H. Choe, and M. Farzan. 2005. Receptor and viral determinants of SARS-coronavirus adaptation to human ACE2. EMBO J. 24:1634–1643.
25. Ligon, B. L. 2006. Reemergence of an unusual disease: the chikungunya epidemic. Semin. Pediatr. Infect. Dis. 17:99–104.
26. Marra, M. A., S. J. Jones, C. R. Astell, R. A. Holt, A. Brooks-Wilson, Y. S. Butterfield, J. Khattra, J. K. Asano, S. A. Barber, S. Y. Chan, A. Cloutier, S. M. Coughlin, D. Freeman, N. Girn, O. L. Griffith, S. R. Leach, M. Mayo, H. McDonald, S. B. Montgomery, P. K. Pandoh, A. S. Petrescu, A. G. Robertson, J. E. Schein, A. Siddiqui, D. E. Smailus, J. M. Stott, G. S. Yang, F. Plummer, A. Andonov, H. Artsob, N. Bastien, K. Bernard, T. F. Booth, D. Bowness, M. Czub, M. Drebot, L. Fernando, R. Flick, M. Garbutt, M. Gray, A. Grolla, S. Jones, H. Feldmann, A. Meyers, A. Kabani, Y. Li, S. Normand, U. Stroher, G. A. Tipples, S. Tyler, R. Vogrig, D. Ward, B. Watson, R. C. Brunham, M. Krajden, M. Petric, D. M. Skowronski, C. Upton, and R. L. Roper. 2003. The Genome sequence of the SARS-associated coronavirus. Science 300:1399–1404.
27. McRoy, W. C., and R. S. Baric. 2008. Amino acid substitutions in the S2 subunit of mouse hepatitis virus variant V51 encode determinants of host range expansion. J. Virol. 82:1414–1424.
28. Morens, D. M., G. K. Folkers, and A. S. Fauci. 2004. The challenge of emerging and re-emerging infectious diseases. Nature 430:242–249.
29. Nguyen, D. C., T. M. Uyeki, S. Jadhao, T. Maines, M. Shaw, Y. Matsuoka, C. Smith, T. Rowe, X. Lu, H. Hall, X. Xu, A. Balish, A. Klimov, T. M. Tumpey, D. E. Swayne, L. P. T. Huynh, H. K. Nghiem, H. H. T. Nguyen, L. T. Hoang, N. J. Cox, and J. M. Katz. 2005. Isolation and characterization of avian influenza viruses, including highly pathogenic H5N1, from poultry in live bird markets in Hanoi, Vietnam, in 2001. J. Virol. 79:4201–4212.
30. Nicholls, J. M., J. Butany, L. L. Poon, K. H. Chan, S. L. Beh, S. Poutanen, J. S. Peiris, and M. Wong. 2006. Time course and cellular localization of SARS-CoV nucleoprotein and RNA in lungs from fatal cases of SARS. PLoS Med. 3:e27.

31. **Page, R. D.** 1996. TreeView: an application to display phylogenetic trees on personal computers. Comput. Appl. Biosci. **12:**357–358.

32. **Parrish, C. R., and Y. Kawaoka.** 2005. The origins of new pandemic viruses: the acquisition of new host ranges by canine parvovirus and influenza A viruses. Annu. Rev. Microbiol. **59:**553–586.

33. **Pickles, R. J., D. McCarty, H. Matsui, P. J. Hart, S. H. Randell, and R. C. Boucher.** 1998. Limited entry of adenovirus vectors into well-differentiated airway epithelium is responsible for inefficient gene transfer. J. Virol. **72:**6014–6023.

34. **Poon, L. L. M., D. K. W. Chu, K. H. Chan, O. K. Wong, T. M. Ellis, Y. H. C. Leung, S. K. P. Lau, P. C. Y. Woo, K. Y. Suen, K. Y. Yuen, Y. Guan, and J. S. M. Peiris.** 2005. Identification of a novel coronavirus in bats. J. Virol. **79:**2001–2009.

35. **Pyrc, K., B. Berkhout, and L. van der Hoek.** 2007. The novel human coronaviruses NL63 and HKU1. J. Virol. **81:**3051–3057.

36. **Pyrc, K., R. Dijkman, L. Deng, M. F. Jebbink, H. A. Ross, B. Berkhout, and L. van der Hoek.** 2006. Mosaic structure of human coronavirus NL63, one thousand years of evolution. J. Mol. Biol. **364:**964–973.

37. **Ramu, C.** 2003. SIRW: a web server for the Simple Indexing and Retrieval System that combines sequence motif searches with keyword searches. Nucleic Acids Res. **31:**3771–3774.

38. **Roberts, A., C. Paddock, L. Vogel, E. Butler, S. Zaki, and K. Subbarao.** 2005. Aged BALB/c mice as a model for increased severity of severe acute respiratory syndrome in elderly humans. J. Virol. **79:**5833–5838.

39. **Roberts, A., and K. Subbarao.** 2006. Animal models for SARS. Adv. Exp. Med. Biol. **581:**463–471.

40. **Rockx, B., T. Sheahan, E. Donaldson, J. Harkema, A. Sims, M. Heise, R. Pickles, M. Cameron, D. Kelvin, and R. Baric.** 2007. Synthetic reconstruction of zoonotic and early human severe acute respiratory syndrome coronavirus isolates that produce fatal disease in aged mice. J. Virol. **81:**7410–7423.

41. **Rota, P. A., M. S. Oberste, S. S. Monroe, W. A. Nix, R. Campagnoli, J. P. Icenogle, S. Penaranda, B. Bankamp, K. Maher, M. H. Chen, S. Tong, A. Tamin, L. Lowe, M. Frace, J. L. DeRisi, Q. Chen, D. Wang, D. D. Erdman, T. C. Peret, C. Burns, T. G. Ksiazek, P. E. Rollin, A. Sanchez, S. Liffick, B. Holloway, J. Limor, K. McCaustland, M. Olsen-Rasmussen, R. Fouchier, S. Gunther, A. D. Osterhaus, C. Drosten, M. A. Pallansch, L. J. Anderson, and W. J. Bellini.** 2003. Characterization of a novel coronavirus associated with severe acute respiratory syndrome. Science **300:**1394–1399.

42. **Simmons, G., D. N. Gosalia, A. J. Rennekamp, J. D. Reeves, S. L. Diamond, and P. Bates.** 2005. Inhibitors of cathepsin L prevent severe acute respiratory syndrome coronavirus entry. Proc. Natl. Acad. Sci. USA **102:**11876–11881.

43. **Sims, A. C., R. S. Baric, B. Yount, S. E. Burkett, P. L. Collins, and R. J. Pickles.** 2005. Severe acute respiratory syndrome coronavirus infection of human ciliated airway epithelia: role of ciliated cells in viral spread in the conducting airways of the lungs. J. Virol. **79:**15511–15524.

44. **Smith, H. O., C. A. Hutchison III, C. Pfannkoch, and J. C. Venter.** 2003. Generating a synthetic genome by whole genome assembly: phiX174 bacteriophage from synthetic oligonucleotides. Proc. Natl. Acad. Sci. USA **100:**15440–15445.

45. **Song, H. D., C. C. Tu, G. W. Zhang, S. Y. Wang, K. Zheng, L. C. Lei, Q. X. Chen, Y. W. Gao, H. Q. Zhou, H. Xiang, H. J. Zheng, S. W. Chern, F. Cheng, C. M. Pan, H. Xuan, S. J. Chen, H. M. Luo, D. H. Zhou, Y. F. Liu, J. F. He, P. Z. Qin, L. H. Li, Y. Q. Ren, W. J. Liang, Y. D. Yu, L. Anderson, M. Wang, R. H. Xu, X. W. Wu, H. Y. Zheng, J. D. Chen, G. Liang, Y. Gao, M. Liao, L. Fang, L. Y. Jiang, H. Li, F. Chen, B. Di, L. J. He, J. Y. Lin, S. Tong, X. Kong, L. Du, P. Hao, H. Tang, A. Bernini, X. J. Yu, O. Spiga, Z. M. Guo, H. Y. Pan, W. Z. He, J. C. Manuguerra, A. Fontanet, A. Danchin, N. Niccolai, Y. X. Li, C. I. Wu, and G. P. Zhao.** 2005. Cross-host evolution of severe acute respiratory syndrome coronavirus in palm civet and human. Proc. Natl. Acad. Sci. USA **102:**2430–2435.

46. **Stevens, J., O. Blixt, T. M. Tumpey, J. K. Taubenberger, J. C. Paulson, and I. A. Wilson.** 2006. Structure and receptor specificity of the hemagglutinin from an H5N1 influenza virus. Science **312:**404–410.

47. **Towner, J. S., X. Pourrut, C. G. Albarino, C. N. Nkogue, B. H. Bird, G. Grard, T. G. Ksiazek, J. P. Gonzalez, S. T. Nichol, and E. M. Leroy.** 2007. Marburg virus infection detected in a common African bat. PLoS ONE **2:**e764.

48. **Traggiai, E., S. Becker, K. Subbarao, L. Kolesnikova, Y. Uematsu, M. R. Gismondo, B. R. Murphy, R. Rappuoli, and A. Lanzavecchia.** 2004. An efficient method to make human monoclonal antibodies from memory B cells: potent neutralization of SARS coronavirus. Nat. Med. **10:**871–875.

49. **Tumpey, T. M., C. F. Basler, P. V. Aguilar, H. Zeng, A. Solorzano, D. E. Swayne, N. J. Cox, J. M. Katz, J. K. Taubenberger, P. Palese, and A. Garcia-Sastre.** 2005. Characterization of the reconstructed 1918 Spanish influenza pandemic virus. Science **310:**77–80.

50. **van der Hoek, L., K. Pyrc, M. F. Jebbink, W. Vermeulen-Oost, R. J. Berkhout, K. C. Wolthers, P. M. Wertheim-van Dillen, J. Kaandorp, J. Spaargaren, and B. Berkhout.** 2004. Identification of a new human coronavirus. Nat. Med. **10:**368–373.

51. **Walsh, P. D., R. Biek, and L. A. Real.** 2005. Wave-like spread of Ebola Zaire. PLoS Biol. **3:**e371.

52. **Woo, P. C. Y., S. K. P. Lau, C.-M. Chu, K.-H. Chan, H.-W. Tsoi, Y. Huang, B. H. L. Wong, R. W. S. Poon, J. J. Cai, W.-K. Luk, L. L. M. Poon, S. S. Y. Wong, Y. Guan, J. S. M. Peiris, and K.-Y. Yuen.** 2005. Characterization and complete genome sequence of a novel coronavirus, coronavirus HKU1, from patients with pneumonia. J. Virol. **79:**884–895.

53. **Woo, P. C. Y., S. K. P. Lau, C. C. Y. Yip, Y. Huang, H.-W. Tsoi, K.-H. Chan, and K.-Y. Yuen.** 2006. Comparative analysis of 22 coronavirus HKU1 genomes reveals a novel genotype and evidence of natural recombination in coronavirus HKU1. J. Virol. **80:**7136–7145.

54. **Yano, Y., M. Kaneniwa, M. Satomi, H. Oikawa, and S. S. Chen.** 2006. Occurrence and density of Vibrio parahaemolyticus in live edible crustaceans from markets in China. J. Food Prot. **69:**2742–2746.

55. **Yano, Y., M. Yokoyama, M. Satomi, H. Oikawa, and S. S. Chen.** 2004. Occurrence of Vibrio vulnificus in fish and shellfish available from markets in China. J. Food Prot. **67:**1617–1623.

56. **Yount, B., K. M. Curtis, E. A. Fritz, L. E. Hensley, P. B. Jahrling, E. Prentice, M. R. Denison, T. W. Geisbert, and R. S. Baric.** 2003. Reverse genetics with a full-length infectious cDNA of severe acute respiratory syndrome coronavirus. Proc. Natl. Acad. Sci. USA **100:**12995–13000.

57. **Yount, B., R. S. Roberts, L. Lindesmith, and R. S. Baric.** 2006. Rewiring the severe acute respiratory syndrome coronavirus (SARS-CoV) transcription circuit: engineering a recombination-resistant genome. Proc. Natl. Acad. Sci. USA **103:**12546–12551.

58. **Yount, B., R. S. Roberts, A. C. Sims, D. Deming, M. B. Frieman, J. Sparks, M. R. Denison, N. Davis, and R. S. Baric.** 2005. Severe acute respiratory syndrome coronavirus group-specific open reading frames encode nonessential functions for replication in cell cultures and mice. J. Virol. **79:**14909–14922.

59. **Zhu, Z., S. Chakraborti, Y. He, A. Roberts, T. Sheahan, X. Xiao, L. E. Hensley, P. Prabakaran, B. Rockx, I. A. Sidorov, D. Corti, L. Vogel, Y. Feng, J. O. Kim, L. F. Wang, R. Baric, A. Lanzavecchia, K. M. Curtis, G. J. Nabel, K. Subbarao, S. Jiang, and D. S. Dimitrov.** 2007. Potent cross-reactive neutralization of SARS coronavirus isolates by human monoclonal antibodies. Proc. Natl. Acad. Sci. USA **104:**12123–12128.